Human Molecular Genetics, 2004, Vol. 13, No. 18 **2061–2074**
doi:10.1093/hmg/ddh215
Advance Access published on July 14, 2004

Differential expression of a novel ankyrin containing E3 ubiquitin-protein ligase, Hace1, in sporadic Wilms' tumor versus normal kidney

Michael S. Anglesio[1,2], Valentina Evdokimova[1,2], Nataliya Melnyk[1,2], Liyong Zhang[3,4], Conrad V. Fernandez[5], Paul E. Grundy[6], Stephen Leach[7], Marco A. Marra[7], Angela R. Brooks-Wilson[7], Josef Penninger[8] and Poul H.B. Sorensen[1,2,*]

[1]Department of Pathology and [2]Department of Pediatrics, British Columbia Research Institute for Children's and Women's Health, University of British Columbia, Vancouver, BC, Canada V5Z 4H4, [3]Department of Medical Biophysics and [4]Department of Immunology, University of Toronto, Toronto, Ontario, Canada, [5]Department of Pediatrics, IWK Grace Health Centre, Halifax, Nova Scotia, Canada B3L 3G9, [6]Cross Cancer Institute, Edmonton AB, Canada T6G 1Z2, [7]Genome Sciences Centre, British Columbia Cancer Agency, Vancouver, BC, Canada V5Z 4S6 and [8]Institute for Molecular Biotechnology of the Austrian Academy of Sciences, 1030 Vienna, Austria

Received May 7, 2004; Revised and Accepted July 6, 2004

We have analyzed the chromosome 6q21 breakpoint of a non-constitutional t(6;15)(q21;q21) rearrangement in sporadic Wilms' tumor. This identified a novel gene encoding a protein with six N-terminal ankyrin repeats linked to a C-terminal HECT ubiquitin-protein ligase domain. We therefore designated this gene *HACE1* (HECT domain and Ankyrin repeat Containing E3 ubiquitin-protein ligase 1). *HACE1* is widely expressed in human tissues, including mature and fetal kidney. We show that Hace1 protein possesses intrinsic ubiquitin ligase activity, utilizes UbcH7 as a candidate partner E2 enzyme and localizes predominantly to the endoplasmic reticulum. Although the *HACE1* locus was not directly interrupted by the translocation in the index Wilms' case, its expression was markedly lower in tumor tissue compared with adjacent normal kidney. Moreover, *HACE1* expression was virtually undetectable in the SK-NEP-1 Wilms' tumor cell line and in four of five additional primary Wilms' tumor cases compared with patient-matched normal kidney. We found no evidence of *HACE1* mutations or deletions, but hypermethylation of two upstream CpG islands correlates with low *HACE1* expression in tumor samples. Our findings implicate Hace1 as a novel ubiquitin-protein ligase and demonstrate that its expression is very low in primary Wilms' tumors.

INTRODUCTION

Analysis of chromosomal translocations in human malignancies has led to the characterization of numerous genes involved in oncogenesis. For example, numerous translocations have been found to either activate proto-oncogenes or to generate gene fusions encoding dominantly acting chimeric oncoproteins (1). Less commonly, mapping of translocations has highlighted the positions of novel tumor suppressor genes (TSGs) within deletion hotspots of tumors, including the von Hippel Lindau (*VHL*) gene of renal carcinoma (2), the *NF2* gene in neurofibromatosis type 2 (3), the *hSNF5/INI1* gene in malignant rhabdoid tumors (4,5) and the *BCSC-1* locus in breast and other cancers (6).

We recently identified a balanced non-constitutional t(6;15)(q21;q21) translocation in a sporadic Wilms' tumor occurring in a 5-month-old male (7). Although Wilms' tumor is the most common renal neoplasm in children, accounting for ~90% of pediatric kidney tumors and 6% of all childhood cancers, the genetics of sporadic Wilms' tumor remain largely unknown (8). Rearrangements of the 6q21 region have been previously reported in this tumor, including t(5;6)(q21;q21) and t(2;6)(q35;q21) translocations (9–11). LOH of this region appears to be rare in Wilms' tumor (9),

*To whom correspondence should be addressed. Tel: +1 6048752936; Fax: +1 6048753417; Email: psor@interchange.ubc.ca

and there is currently little evidence for a 6q21 Wilms' tumor suppressor locus. However, deletions of 6q21 have been widely reported in human malignancies, including carcinomas of the breast, ovary and prostate, as well as in leukemias and lymphomas (12–15), and this region is hypothesized to harbor one or more TSGs (16). These observations highlight chromosome 6q21 as a region frequently targeted for genomic alterations in human cancer. We therefore postulated that the t(6;15) translocation of the index case might be contributing to Wilms' tumor oncogenesis, either through oncogene activation or by targeting a 6q21 TSGs. This prompted us to search for the 6q21 gene or genes potentially altered by the t(6;15) rearrangement.

In this study, we have characterized the 6q21 region interrupted by the Wilms' tumor t(6;15) translocation. We report that the 6q21 breakpoint maps to a non-coding region with >200 kb from the nearest known gene, but ~50 kb upstream of a novel open reading frame (ORF). This ORF encodes a protein with a previously unreported domain architecture consisting of six ankyrin repeats linked to a HECT (homologous to E6-AP C-terminus) domain. HECT domains have thus far only been described in E3 ubiquitin-protein ligases (17,18). E3 ligases are essential components of a highly conserved pathway involving conjugation of one or more ubiquitin (Ub) polypeptides to specific substrate proteins, leading in most cases to substrate proteasomal degradation (17,19). We therefore designated this gene *HACE1* (HECT domain and Ankyrin repeat Containing E3 ubiquitin-protein ligase 1). Hace1 protein has *in vitro* and *in vivo* ubiquitin ligase activity and represents, to our knowledge, the first documented example of a HECT domain containing ubiquitin ligase possessing N-terminal ankyrin repeats. We found that although *HACE1* is ubiquitously expressed in normal tissues, including both adult and fetal kidneys, mRNA and protein levels were almost undetectable in the index case and in four of five institutional Wilms' tumor cases compared with matching adjacent normal kidney, and in the SK-NEP-1 Wilms' tumor cell line. Lower expression was strongly associated with hypermethylation of two CpG islands located upstream of the *HACE1* locus. Our findings implicate Hace1 as a novel HECT E3 ubiquitin-protein ligase whose lack of expression is associated with sporadic Wilms' tumor.

RESULTS

Mapping the 6q21 breakpoint in Wilms' tumor

To assess candidate genes potentially affected by the t(6;15)(q21;q21) translocation in the index case, we focused on the 6q21 breakpoint as this region has previously been implicated in Wilms' tumors and other human malignancies. Using 6q21 bacterial artificial chromosomes (BACs) for fluorescence *in situ* hybridization (FISH), we identified several overlapping BACs that spanned the translocation breakpoint (i.e. that showed three signals as opposed to the normal two; Fig. 1A). On the basis of sequence information from NCBI (http://www.ncbi.nlm.nih.gov) and UCSC (http://genome.ucsc.edu) genome databases, we assembled a precise map of the involved 6q21 region and narrowed the breakpoint to an ~12 kb region between the D6S2097 and STSG6084 polymorphic markers (Fig. 1C). We next determined the restriction enzyme distribution within this region from publicly available genomic sequences. Southern blotting using genomic DNA from the index case and the SB1 probe (Fig. 1C) allowed us to confirm the position of the 6q21 breakpoint, as rearrangements were detected in the tumor sample but not in matched normal tissue or control samples (shown for *Pst*I digests in Fig. 1B).

Identification of the *HACE1* gene

Using public database sequences, we next inspected the region surrounding the 6q21 breakpoint for candidate genes potentially affected by the rearrangement. No previously characterized genes were present in this region. We therefore used GenScan gene prediction software to search for novel ORFs. No coding sequences were identified spanning the breakpoint, indicating that the translocation does not directly disrupt a gene in the 6q21 region. However, a novel 2727 bp ORF located ~50 kb downstream was identified by this strategy, a portion of which matched to the 5′ end of a non-annotated, IMAGE Consortium expressed sequence tag (EST; GenBank accession no. BC034982). We obtained this cDNA clone and sequenced it in its entirety, revealing 100% sequence identity with the predicted full-length ORF from 6q21. Alignment to publicly available 6q21 genomic sequences using the UCSC genome browser BLAT tool predicts that this ORF is organized into 24 exons (Fig. 1C). The nearest known gene, *BVES* (blood vessel epicardial substance), lies ~200 kb upstream of the breakpoint (Fig. 1C).

Protein domain analysis predicted that the 6q21 ORF encodes a 909 amino acid protein (~103 kDa) possessing six N-terminal ankyrin repeats and a C-terminal HECT domain (Fig. 1D). Ankyrin repeats are well-documented to mediate protein–protein interactions (20), whereas HECT is a catalytic domain possessing ubiquitin-protein ligase activity (17,18,21). We therefore designated this gene *HACE1*. Comparison of the Hace1 protein sequence to public databases using NCBI BLAST and DART tools (http://www.ncbi.nlm.nih/BLAST) highlights Hace1 as the first documented example of an E3 ligase in which a HECT domain is linked to ankyrin repeats. Interestingly, when the *HACE1* coding sequence was aligned with those of other genomes using the BLAT tool at the UCSC genome database (http://genome.ucsc.edu), orthologues of *HACE1* appear to be present only in vertebrate species (data not shown). Hace1 ankyrin repeats show >47% sequence similarity with those of the cyclin-dependent kinase inhibitors p16INK4A and p19INK4D (Fig. 1D), both of which are known to be inactivated in human malignancies including Wilms' tumor (22). The Hace1 HECT domain is also highly conserved, with more than 53% sequence similarity to the HECT domains of well-characterized ubiquitin ligases including E6-AP, which destabilizes p53 in HPV infected cervical carcinoma cells (23), Nedd4, which regulates stability of the epithelial Na+ channel (ENaC) and insulin-like growth factor 1 receptor (21), and Smurf 1 and 2, which are involved in ubiquitination of TGF-β receptors (24). HECT family E3 ligases are known to contain an invariant C-terminal cysteine residue necessary

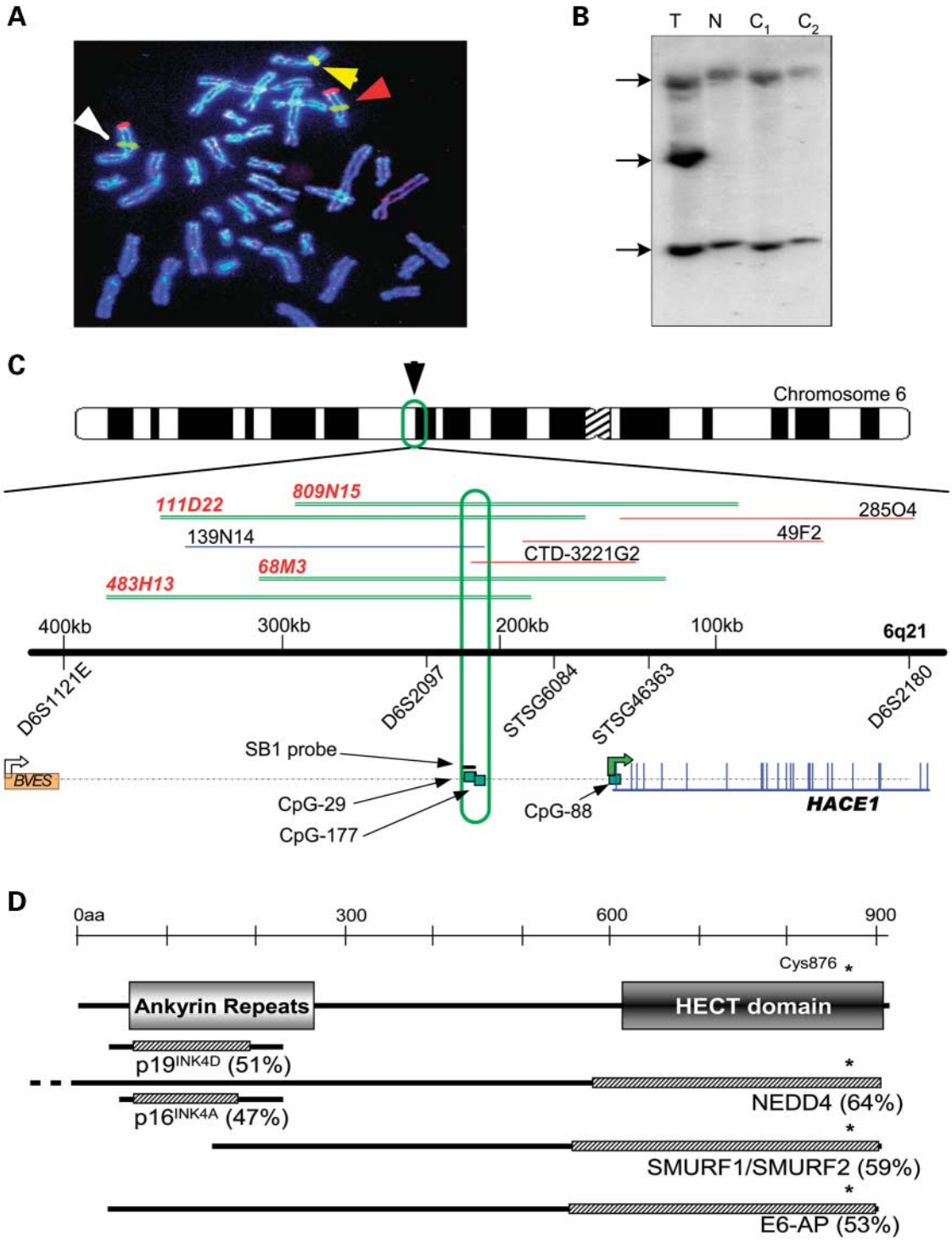

Figure 1. Identification of a novel gene, *HACE1*, within the t(6;15)(q21;q21) breakpoint region in the Wilms' tumor index case. (**A**) FISH using 6q21 BAC probe *809N15* (green) and a telomeric probe for 6q (red). Normal Chr 6 (white arrow), derivative Chr 15 (red arrow) and derivative Chr 6 (yellow arrow) are indicated. (**B**) Southern blotting using SB1 probe indicated in (B) demonstrates re-arrangement in *Pst*I digested genomic DNA from the index tumor (T) case but not in peripheral blood (N) or control samples (C_1 and C_2). (**C**) Mapping of the 6q21 breakpoint region. Twenty-four exon structure of *HACE1* as predicted by the UCSC genome browser BLAT tool is shown. BACs used for mapping of the breakpoint region were identified using Finger printed contigs (FPC) software and sequence information from the NCBI and UCSC genome databases and are indicated as follows: BACs spanning the t(6;15)(q21;q21) breakpoint (double green lines); BACs that remain on the derivative Chr 6 (red single lines); BACs detected on the derivative 15 (blue single line), green boxes denote CpG islands. **(D)** Hace1 (GenBank accession number AAH34982) consists of six N-terminal ankyrin repeats and a C-terminal HECT domain as predicted by Pfam and SMART database tools. An invariant Cys residue in the HECT domain is indicated by asterisk. Alignment to a number of proteins containing ankyrin repeats or HECT domains are shown below; hashed region corresponds to the region of significant similarity. Percentage similarity was calculated using BLAST tools.

for thioester bond formation with ubiquitin (18); in Hace1 this appears to be represented by Cys-876 (Fig. 1D).

Normal *HACE1* expression patterns

We next examined *HACE1* expression profiles in normal human tissues by northern analysis. Using a full-length cDNA probe, we found that human *HACE1* is expressed as a single mRNA species of ~4.6 kb in multiple tissues, including strong expression in heart, brain and kidney (Fig. 2A). As Wilms' tumor is hypothesized to derive from early metanephrogenic stem cells (25–28), we also assessed *HACE1* expression in three (day 54–122) human fetal kidney tissue samples. We found that, although variable, mRNA transcripts are expressed in these cells at levels that are similar to or greater than in mature pediatric kidney (Fig. 2B). There was no obvious trend in expression patterns with the age of the human fetal kidney samples, although this requires a larger sample size for rigorous evaluation. To examine expression of Hace1 protein, we generated polyclonal α-Hace1 antibodies directed towards either the second ankyrin repeat or to full-length recombinant protein. Both antibodies detect a protein with the expected size of 103 kDa identical to that of recombinant Hace1 in both fetal and pediatric kidney cells, as well as in the HEK293 human embryonic kidney cell line (Fig. 2C).

Hace1 possesses ubiquitin ligase activity *in vitro* and *in vivo*

To determine whether Hace1 possesses a ubiquitin ligase activity, we tested the ability of this protein to form a thioester bond with ubiquitin, a well-documented characteristic of HECT E3 ligases (17). *In vitro* [^{35}S]-labeled Hace1 was incubated in the presence of GST–Ub and E1 Ub-activating enzyme, along with a panel of E2 Ub-conjugating enzymes (Fig. 3A). As HECT domains contain a conserved Cys residue which is crucial for Ub transfer to substrate proteins, we mutated Cys-876 to Ser and tested this Hace1-C876S mutant in thioester bond formation. As seen in Figure 3A (top panel), an additional higher molecular mass band corresponding to the expected size of a Hace1–GST–Ub conjugate (~140 kDa) was evident in the presence of the UbcH7 E2 enzyme (lane 8). Thioester bond formation was completely abolished by the C876S substitution in Hace1 (Fig. 3A, bottom panel) or by disulphide bond reducing agent β-mercaptoethanol (Fig. 3B; compare lanes 1 and 4), indicating specificity of the reaction. These data confirm Hace1 ubiquitin ligase activity *in vitro* and identify UbcH7 as a candidate partner E2.

To demonstrate the involvement of Hace1 in the ubiquitination of proteins *in vivo*, HA-tagged Hace1 was stably expressed in NIH3T3 fibroblasts (Fig. 3C). Cytoplasmic extracts from these cells were then subjected to immunoprecipitation with α-HA antibodies followed by western blotting with α-Ub antibodies to assess whether Hace1 associates with ubiquitinated proteins. As shown in Figure 3D, overall levels of protein ubiquitination were similar in HA–Hace1 and vector alone cells. However, high molecular weight ubiquitinated proteins could only be detected in α-HA immunoprecipitates from the HA–Hace1 expressing cells (compare lanes 3 and 4). The level of ubiquitinated proteins in these immunoprecipitates was increased in the presence of

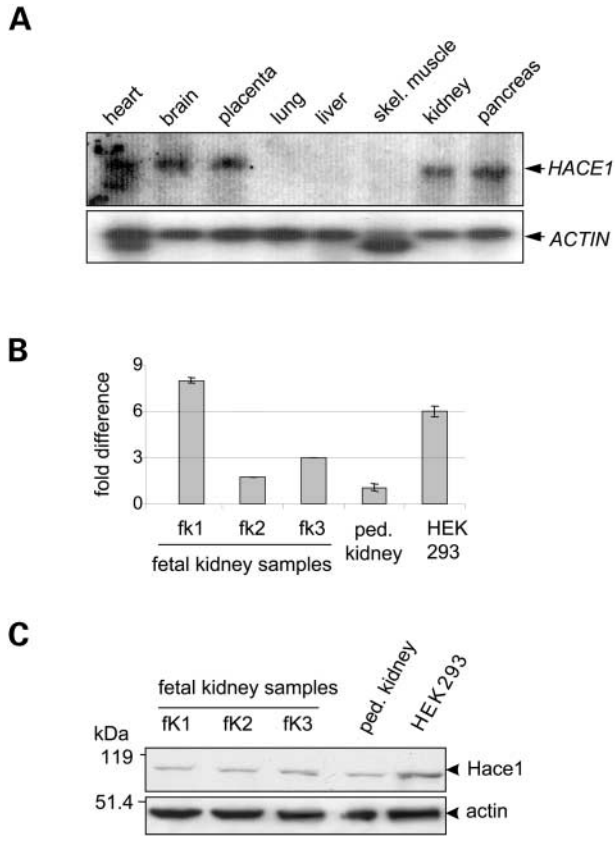

Figure 2. Hace1 expression in normal tissues. (**A**) Northern blotting demonstrating *HACE1* mRNA expression in a panel of normal tissues. Membrane was probed with the full-length Hace1 cDNA. (**B**) qRT–PCR showing *HACE1* expression in three normal fetal kidney samples (fk1–3), pediatric (ped.) kidney and HEK293 (human embryonic kidney) are shown for comparison. Expression of *HACE1* is normalized to the ped. kidney sample. (**C**) Western blotting showing Hace1 protein expression fetal kidney samples [from (B)]. Actin serves as a loading control (lower panel).

proteasome inhibitors such as lactacystin or MG132 (data not shown), indicating that at least some of the proteins targeted for ubiquitination by Hace1 are normally degraded by the proteasome. Moreover, we found that Hace1 directly interacts with the 26S proteasomal complex as Hace1 could be immunoprecipitated using antibodies against the 20S core proteasomal subunits (Fig. 3E, lane 3). Although the identity of Hace1 target proteins in the earlier mentioned immunoprecipitates remains to be established, our data strongly support the involvement of Hace1 in ubiquitination and degradation of cellular proteins.

Subcellular localization of Hace1

To further characterize Hace1, we analyzed its localization within the cell. Subcellular fractionation followed by western blotting demonstrated that in exponentially growing NIH3T3 fibroblasts both endogenous and ectopically expressed Hace1 are found predominantly in the endoplasmic reticulum (ER) and the cytoplasm, although a small amount of endogenous protein is also present in other fractions (Fig. 4A). ER localization was confirmed by co-immunostaining of

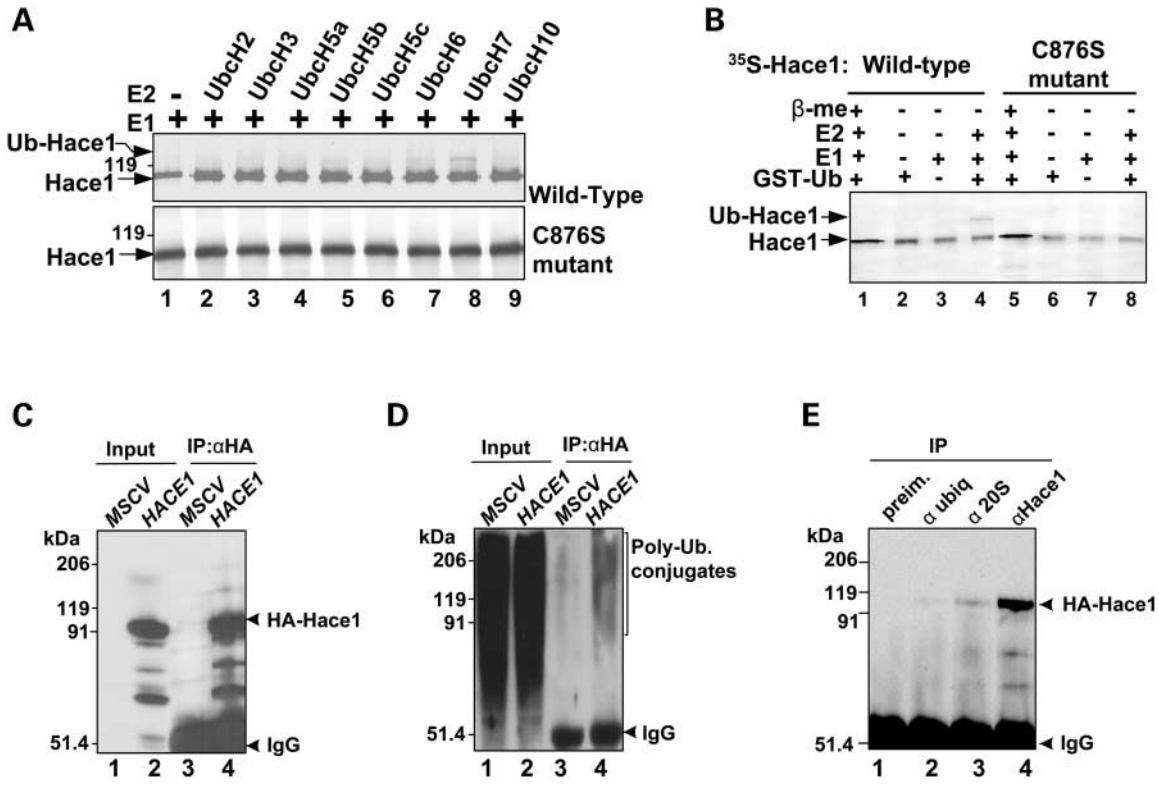

Figure 3. Hace1 exhibits E3 ubiquitin ligase activity *in vitro* and *in vivo.* (**A**) Thioester bond formation assay was performed using the [^{35}S]-methionine labeled wild-type or C876S point-mutant Hace1 proteins, GST-Ub, E1 activating enzyme and the respective E2s, as indicated. After 30 min at 30°C, the reactions were stopped with SDS–PAGE sample buffer without β-mercaptoethanol and subjected to SDS–7% PAGE and autoradiography. (**B**) The reactions were carried out as in (A) except that exclusively UbcH7 has been used as a source of E2. Reactions were stopped with or without β-mercaptoethanol. Note that addition of β-mercaptoethanol (lane 1) or mutation of the invariant Cys residue (lane 8) completely abolished thioester formation. (**C** and **D**) Cytosolic extracts from NIH3T3 cells ectopically expressing HA-Hace1 or vector alone were used for immunoprecipitation (IP) with α-HA antibodies. Of the IP fractions 20% were then subjected to SDS–7% PAGE and western blotting with α-HA (C) or α-Ub (D) antibodies. Input fraction lanes represent 5% of cytosolic cell extract used for IP. (**E**) Cytosolic extracts obtained from NIH3T3 cells expressing HA–Hace1 were used for IP with either rabbit pre-immune, α-Ub, α-Hace1 or α-20Sα and β proteasomal subunits antibodies, as indicated. Immunoprecipitated proteins were then separated by SDS–7% PAGE and analyzed by western blotting using α-HA antibodies.

Hace1 with the ER resident, BiP (Grp78). As seen in Figure 4B, a predominantly perinuclear reticular staining pattern of the ER and of the nuclear envelop was observed for both Hace1 and BiP in NIH3T3 cells using immunofluorescence microscopy. This suggests that a significant portion of Hace1 localizes to the ER.

Altered expression of *HACE1* in sporadic Wilms' tumor

As the 6q21 breakpoint in the index case occurred ∼50 kb upstream of the *HACE1* locus, we hypothesized that *HACE1* expression might be affected by the t(6;15) translocation. Moreover, we wondered whether altered *HACE1* expression might represent a recurrent molecular alteration in sporadic Wilms' tumor. To begin to address this possibility, we assessed *HACE1* mRNA levels in the index case and in five additional institutional Wilms' tumor cases with patient-matched adjacent normal kidney by quantitative RT–PCR (qRT–PCR). The histology of each tumor sample confirmed the presence of at least 80% tumor cells (data not shown). Of the six paired samples, five tumor specimens showed markedly lower *HACE1* mRNA expression compared with their matching normal kidney counterparts, including the index case (Fig. 5A). Although there was variability in the absolute degree to which *HACE1* expression was lower, the average decrease in transcript levels was ∼5-fold. Low expression was confirmed at the protein level by western blotting using α-Hace1 antibodies (Fig. 5B), as expression of Hace1 protein was very low or undetectable in the index case and in the other four cases with low mRNA levels, compared with matching normal kidney. We next assessed *HACE1* expression levels and the presence of variant transcripts in the SK-NEP-1 Wilms' tumor cell line by northern analysis. Transcript levels are virtually undetectable in these cells compared with HEK293 human embryonic kidney cells or Ewing tumor and rhabdomyosarcoma cell lines (Fig. 5C). Hace1 mRNA expression was also low to non-detectable in neuroblastoma cell lines. In agreement with these findings, Hace1 protein levels are extremely low in SK-NEP-1 and neuroblastoma cell lines compared with HEK293, Ewing tumor and rhabdomyosarcoma cells (Fig. 5D).

Absence of *HACE1* mutations or deletions in sporadic Wilms' tumor

Current views hold that Wilms' tumor most likely derives from embryonic kidney (26–28). As we observed strong

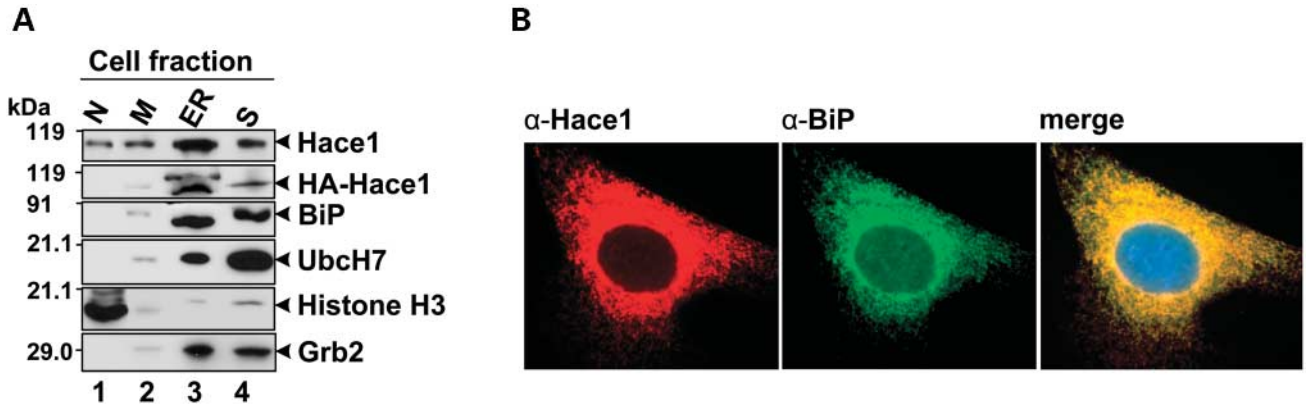

Figure 4. Hace1 is mainly localized to the ER. (**A**) Subcellular fractionation of NIH3T3 cell extract. Equal amounts (50 μg) of nuclear (N), mitochondrial (M), endoplasmic reticulum/polyribosome (ER) and cytosolic (S) fractions were analyzed by western blotting using the respective antibodies, as indicated. Histone H3, BiP and Grb2 were used as markers of nuclear, ER and cytosolic fractions, respectively. (**B**) Indirect immunofluorescence microscopy of NIH3T3 cells using α-Hace1 (red) and BiP (green) antibodies, as indicated. Nuclear staining by propidium iodide is in blue.

Hace1 expression in both mature pediatric and fetal kidneys but not in most of the Wilms' tumors analyzed, one possibility is that Hace1 down regulation or inactivation is a common and potentially etiologic event in this disease. However, it is equally plausible that the specific (as yet unknown) blastemal cell giving rise to Wilms' tumor does not express *HACE1* and that the observed lack of expression simply reflects the normal expression profile of the putative neoplastic precursor cell. We therefore assessed the Wilms' tumor cohort for potential genetic mechanisms of *HACE1* down regulation as a strategy for distinguishing between these possibilities, as loss of TSGs in malignancies typically involves inactivation of both the alleles (29). Current literature indicates that chromosomal rearrangements, large scale deletions or LOH of the 6q21 region are rare in Wilms' tumor (8–11). Unfortunately, aside from the index case, karyotypes were not available for the Wilms' tumors analyzed in this study. To search for alternative mechanisms that might underlie altered *HACE1* expression in Wilms' tumor, we screened the cohort of cases and matched normal kidney as well as the SK-NEP-1 cell line for *HACE1* mutations. All exons and intron–exon boundary regions were sequenced from genomic DNA of each sample. No sequence discrepancies between tumor and normal DNAs were found for any of the six cases. Furthermore, no mutations were found in the SK-NEP-1 cell line. Sequence data were compared with the UCSC human genome database and a total of eight *HACE1* polymorphisms were identified in the earlier mentioned cohort (Supplementary Material, Table S1). Two of the polymorphisms were within the coding sequences, but only one represents an amino acid change. However, the latter (Asp to Gly at amino acid 399) does not affect any identifiable functional domains within Hace1 protein, and when a non-disease control cohort of 95 individuals was tested for this polymorphism it was present in 1% of samples. Therefore, it most likely represents a low-frequency polymorphism in the general population. Of the five Wilms' tumor cases with low *HACE1* expression, at least one heterozygous polymorphism was found in four of the tumor (and normal) DNAs as well as in the SK-NEP-1 cell line, suggesting that LOH of the *HACE1* locus is unlikely in this cohort. However, our sequencing strategy cannot rule out micro-deletions of exons or other genomic sequences located between these polymorphisms. Therefore, our data indicate that a genetic mechanism involving point mutations or deletions is unlikely to explain the low *HACE1* expression observed in Wilms' tumor, although larger numbers of cases must be assessed to rigorously test this assumption.

Upstream CpG island methylation is associated with low *HACE1* expression

Recent studies indicate that promoter hypermethylation may be as frequent as inactivating mutations for reducing TSG expression in human malignancies (30). Methylation involves the addition of methyl groups to cytosine residues within CpG islands within coding or non-coding sequences of genetic loci, generally resulting in gene silencing (31,32). We therefore investigated the methylation status of CpG islands at the *HACE1* locus in the primary Wilms' tumor cohort and in the SK-NEP-1 cell line. There are three CpG islands located within or near the *HACE1* locus, one at the promoter extending into exon 1 which contains 88 CG dinucleotides (CpG-88), and two located ~50 kb upstream of the Hace1 transcriptional start site containing 177 (CpG-177) and 29 (CpG-29) CG dinucleotides repeats, respectively (Fig. 1C). To assess whether altered methylation might influence *HACE1* expression, we analyzed methylation status at each of these CpG islands by digestion with the methylation sensitive restriction enzymes *Hae*II, *Hpa*II or *Bss*HII, followed by semi-quantitative PCR (Fig. 6A). No evidence of methylation at CpG-88 was found in any of the tumor or normal kidney samples (Fig. 6A). However, hypermethylation of either CpG-177 and CpG-29, or both, was observed in four out of five Wilms' tumors with low *HACE1* mRNA expression (Fig. 6A) as well as in SK-NEP-1 cells (Fig. 6B). It was never observed in any of the normal kidney samples (data not shown).

If hypermethylation of CpG-29/CpG-177 is mechanistically related to low *HACE1* expression, then pharmacological demethylation of these islands would be expected to restore

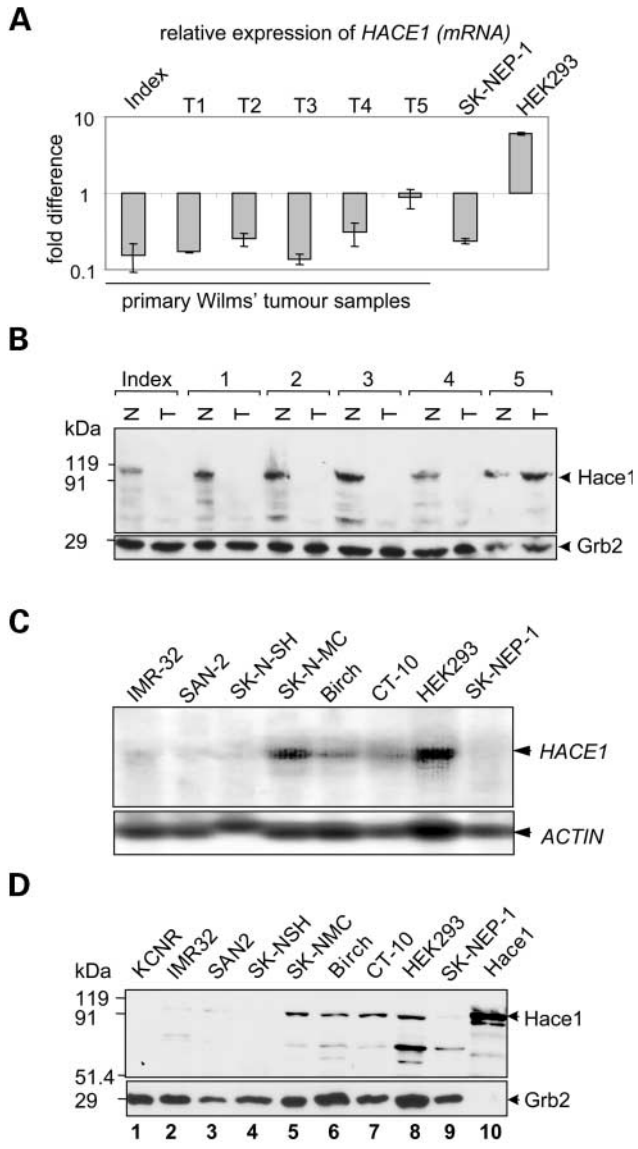

Figure 5. Hace1 expression in Wilms' tumors and pediatric cancer cell lines. (**A**) qRT–PCR showing expression of *HACE1* mRNA in Wilms' tumor samples relative to patient-matched normal kidney. *HACE1* expression relative to a normal pediatric kidney sample is shown for SK-NEP-1 and HEK293 (human embryonic kidney) cells. (**B**) Western blotting for the Hace1 protein showing the tumor (T) samples [from (A)] patient-matched normal kidney (N). (**C**) Northern blotting demonstrating *HACE1* mRNA expression in a panel of pediatric tumor cell lines including neuroblastomas (SAN-2, IMR-32, SK-N-SH), Ewing's sarcoma (SK-N-MC), rhabdomyosarcomas (Birch, CT-10), Wilms' tumor (SK-NEP-1) and HEK293 cells. Membranes were probed with the full-length Hace1 cDNA. (**D**) Western blotting showing Hace1 protein expression in pediatric tumor cell lines [from (C), and an additional neuroblastoma line, KCNR]. Westerns were done using the N-terminal α-Hace1 antibody. Recombinant Hace1 protein (lane 10) is used to confirm the specificity of the antibody. Grb2 serves as a loading control.

expression levels. As SK-NEP-1 Wilms' tumor cells express extremely low *HACE1* levels and both CpG-29 and CpG-177 are methylated in this line, we treated cells with the methylation inhibitor 5-aza-2-deoxycytidine (5AZ) (33,34) and assessed effects on *HACE1* expression. As shown in Fig. 6B, treatment with this agent reduced methylation at both CpG-29 and CpG-177, particularly at 5 μM 5AZ. Moreover, this was associated with at least a 4-fold increase in *HACE1* mRNA expression in the presence of 5 μM 5AZ (Fig. 6C). These findings strongly suggest that methylation status of CpG-29 and CpG-177 influences *HACE1* expression. To examine the functional consequences of this observation, we next performed chromatin immunoprecipitation (ChIP) to analyze whether the *HACE1* locus exists in an active or inactive chromatin conformation in SK-NEP-1 cells. This was assessed by comparing the relative levels of acetylated-histone H3 versus dimethyl-(Lys79)-histone H3 bound to the *HACE1* promoter. Acetylated-histone H3 is known to associate with DNA of active chromatin, whereas dimethyl-(Lys79)-histone H3 correlates with chromatin present in the inactive conformation of heterochromatin or silenced genes (35–37). As shown in Figure 6D, the promoter region of the *HACE1* gene exists predominantly in an inactive chromatin conformation in normally growing SK-NEP-1 cells (i.e. associated with dimethyl-(Lys79)-histone H3 by ChIP). However, treatment with 5 μM 5AZ reverses this pattern, switching the *HACE1* promoter to an active chromatin conformation associated predominantly with the acetylated-histone H3. As a control, we performed identical studies with HEK293 cells (Fig. 6D, left panel) which abundantly express *HACE1* (Fig. 4). Consistent with its high expression, the *HACE1* locus exists in an active chromatin organization in these cells, and no change in chromatin structure is evident after treatment with 5AZ. Taken together, our data are consistent with a role for CpG-29 and CpG-177 hypermethylations in influencing *HACE1* expression, although additional studies are required to confirm this possibility and whether it represents an acquired alteration in tumor cells versus the normal pattern of methylation in the Wilms' tumor neoplastic precursor cell.

DISCUSSION

In this study, we demonstrate that a previously uncharacterized E3 ubiquitin-protein ligase gene is located ~50 kb downstream of the 6q21 breakpoint of a t(6;15) translocation in sporadic Wilms' tumor. This gene, which we designated *HACE1*, encodes a 103 kDa protein containing six N-terminal ankyrin repeats connected via a linker region to a C-terminal HECT domain. The latter has to date only been described in E3 ligases (17), implicating the Hace1 protein as a new member of the HECT family of E3 ubiquitin-protein ligases. The protein ubiquitination process involves a highly conserved pathway in which one or more Ub polypeptides become conjugated to specific substrate proteins (17,19). This multistep process involves a cascade of three different classes of enzymes. An ATP-dependent Ub-activating E1 enzyme first forms a thioester bond with Ub, and then transfers the activated Ub moiety to one of a number of different E2 Ub-conjugating (Ubc) enzymes. Finally, E3 ubiquitin ligases catalyze the transfer of Ub from the cognate E2 to a lysine on the substrate protein. Binding of substrate proteins appears to be mediated by the N-terminal protein–protein interaction domains of E3 ligases (17,18,21).

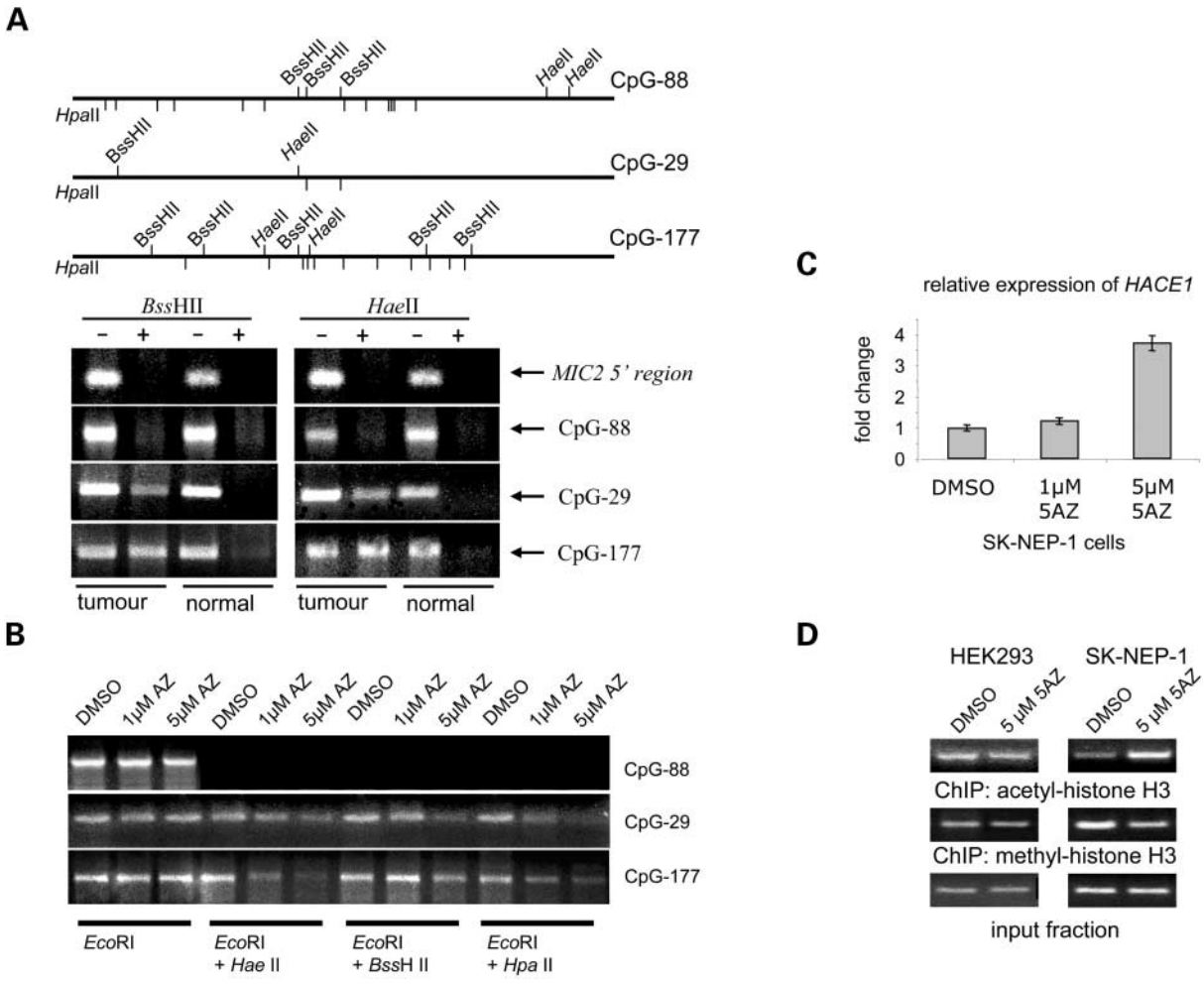

Figure 6. Methylation analysis of the *HACE1* gene in Wilms' tumor patient's samples and SK-NEP-1 cell line. (**A**) Representative sample: Wilms' tumor and patient-matched normal kidney DNA was digested using *EcoR*I in combination with *Hae*II, *Hpa*II or *Bss*HI methylation sensitive restriction enzymes (upper panel illustrates restriction map of each PCR amplicon), methylation of three CpG islands surrounding the *HACE1* locus was then assessed by semi-quatitative PCR. Note that hypermethylation was restricted exclusively to tumor samples in CpG-29 and CpG-177 islands, no methylation was observed at CpG-88. (**B**) SK-NEP-1 Wilms' tumor cells were treated with 5AZ to inhibit methylation. Semi-quantitative PCR was then used to assess methylation status of CpG islands associated with *HACE1* as described in (A). After treatment with 5AZ, methylation of CpG-29 and CpG-177 islands is decreased, whereas there is no evidence of methylation at CpG-88. Similar results were observed in three independent experiments. (**C**) qRT–PCR showing an increase in *HACE1* mRNA transcripts upon treatment of SK-NEP-1 cells with increasing doses of 5AZ. A maximal response was observed at 5 μM 5AZ. (**D**) ChIP assays to detect active or inactive chromatin were performed using antibodies against either acetyl-histone H3 (acetyl H3) or dimethyl-(Lys79)-histone H3 (methyl H3), respectively. SK-NEP-1 and HEK293 cells treated with or without 5 μM 5AZ prior to ChIP studies. PCR products in the top two panels for each cell line correspond to the transcriptional start of *HACE1* and is overlapped by CpG-88. Identical results were observed in four independent experiments.

HACE1 is widely expressed in human tissues, including both fetal and mature kidneys. The Hace1 protein forms thioester bonds with ubiquitin as expected for a HECT family E3 ligase (17,18), and is associated with high molecular weight ubiquitinated proteins within cells. Among a panel of E2 ubiquitin carrier proteins, thioester bond formation *in vitro* occurred in the presence the UbcH7 E2 enzyme, and weakly with UbcH6 and UbcH5b, all of which are common partners of other HECT domain containing E3 ubiquitin-protein ligases. We also found that Hace1 associates with ubiquitinated proteins and components of the 26S proteasomal complex, indicating that at least some of the proteins targeted for ubiquitination by Hace1 are likely to be degraded by the proteasome. Using cell fractionation and immunofluorescence microscopy, we found that Hace1 localizes predominantly to the ER indicating its possible involvement in ER-associated protein degradation (ERAD). ERAD is a quality control process that selectively directs degradation of misfolded and aberrant proteins through ubiquitination within the ER followed by transport to the proteasome (17,38). More studies are necessary to demonstrate whether Hace1 contributes to this process.

Most HECT E3 ligases characterized to date contain N-terminal WW domains for substrate interaction and targeting (17,18,21). In fact, the presence of ankyrin repeats within an E3 ligase as in Hace1 has not been previously described. Given this modular structure, Hace1 may represent a novel sub-family of HECT E3 ubiquitin-protein ligases.

Ankyrin motifs are well known to mediate protein–protein interactions (20), and therefore likely serve the same function in Hace1. Alternatively, the ankyrin repeats may be necessary for Hace1 to link with non-substrate proteins in higher order signaling complexes, a function that has been described previously for ankyrin motifs (20,39). Interestingly, the Hace1 ankyrin repeats show high sequence similarity to those of the cyclin-dependent kinase inhibitors p16INK4A (CDKN2A) and p19INK4D (CDKN2D), which inhibit the cell cycle by binding to and inhibiting CDK4 and CDK6.

HACE1 expression was very low both at the mRNA and protein levels in five of the six sporadic Wilms' tumors compared with patient-matched normal kidney, including the index case. Moreover, expression of this gene is virtually undetectable in SK-NEP-1 Wilms' tumor cells. This raises the possibility that loss of *HACE1* expression may be a recurrent alteration in Wilms' tumor, and that *HACE1* inactivation plays a role in the pathogenesis of Wilms' tumor. On the other hand, this may reflect the normal expression profile of *HACE1* in the Wilms' tumor neoplastic precursor cell; i.e. *HACE1* may not normally be expressed in the putative blastemal cell of origin of this disease. Typically, inactivation of TSGs in human malignancies involves targeting of both alleles by genetic or epigenetic mechanisms (29). Therefore, we searched for mechanistic evidence of *HACE1* inactivation in Wilms' tumor. As chromosomal translocations or other cytogenetic abnormalities involving 6q21 have only infrequently been reported in Wilms' tumors (7,9–11), this is unlikely as a mechanism of *HACE1* loss. Moreover, in the index case of the present study the 6q21 breakpoint did not directly disrupt the *HACE1* gene, but occurred outside of the coding region. We also failed to detect *HACE1* mutations in any of the cases with low *HACE1* expression, and LOH of this gene was not evident by analysis of several informative markers identified within the *HACE1* locus. The latter is consistent with other studies indicating that LOH of 6q21 is rare in Wilms' tumor (9). Although further studies using larger case cohorts to definitively rule out that mutations or deletions of *HACE1* occur in sporadic Wilms' tumor, our results to date do not support a role for genetic mechanisms in HACE1 loss in Wilms' tumor.

Gene inactivation by methylation appears to be at least as frequent as inactivating mutations for disrupting TSG expression in sporadic tumors (30). For example, in sporadic breast and ovarian carcinomas, *BRCA1* mutations are highly infrequent and epigenetic silencing by promoter methylation is the only apparent mechanism for loss of function in most cases (40). We therefore examined whether the CpG islands associated with the *HACE1* locus were differentially methylated in tumor versus normal kidney samples. Although the *HACE1* promoter CpG island was not methylated, we detected hypermethylation of CpG-29 and CpG-177, located ~50 kb upstream of *HACE1* exon 1, in four of the five Wilms' tumors with reduced mRNA expression, and also in the SK-NEP-1 cell line. Moreover, treatment with the methyltransferase inhibitor 5AZ not only blocked methylation of these islands but also restored *HACE1* mRNA expression in SK-NEP-1 cells. One obvious caveat of these experiments is that 5AZ as a pharmacological inhibitor has a global effect on CpG methylation. We therefore performed ChIP analysis of the *HACE1* promoter region using antibodies to acetylated-histone H3 or dimethyl-(Lys79)-histone H3, which associate with actively transcribed versus inactive, silenced chromatin, respectively (36,37). These experiments indicated that 5AZ treatment of SK-NEP-1 cells shifts the *HACE1* promoter from an inactive chromatin conformation to that of active chromatin, in keeping with the increased expression of this gene in response to 5AZ. In contrast, the *HACE1* promoter of HEK293 human embryonic kidney cells, which express high levels of *HACE1*, exists in an active conformation under normal growth conditions and there is no change in chromatin structure upon treatment with 5AZ. These findings provide compelling evidence that *HACE1* expression is influenced by upstream CpG island methylation. It is important to note, however, that our findings do not establish whether the correlation between CpG island hypermethylation and low *HACE1* expression is specific to transformed cells. That is, they do not distinguish between acquired hypermethylation leading to *HACE1* inactivation as an etiologic event in Wilms' tumor oncogenesis, versus hypermethylation leading to low *HACE1* expression as part of the normal transcriptional regulation of this gene in the Wilms' tumor precursor cell. Functional studies are necessary to determine whether the Hace1 protein has suppressive effects on cell growth, and whether its loss contributes to Wilms' tumor oncogenesis.

Although methylation of CpG dinucleotides outside of promoters has been documented to influence gene transcription (41), most studies which describe epigenetic silencing of genes have focused on CpG islands located within promoters or coding regions of genes (30). Recently, distance effects on insulator methylation were reported for the *H19* gene, whereby imprinting by CpG methylation at more distant sites regulated mono-allelic expression of both *H19* and *Igf2* (42,43). In addition, reduced expression of Sonic hedgehog (*SHH*) has been associated with chromosomal rearrangements occurring 15–250 kb from the *SHH* locus in holoprosencephaly (44,45). It is possible that long distance effects of CpG island methylation on transcription may be a more general mechanism for gene silencing in human cancers. This might explain how chromosomal translocation breakpoints located at long distances from promoters of potential TSGs could influence gene silencing. It is well-documented that heterochromatin has a silencing effect on adjacent euchromatin, likely through spreading of histone methylation (46–48). It is possible that by juxtaposing heterochromatin in the vicinity of potential TSGs, a chromosomal translocation can exert long distance transcriptional suppression on that locus by effecting local methylation changes. For the index case in this study, the 6q21 breakpoint mapped very closely to if not within CpG-29 or CpG-177. Moreover, both of these islands were methylated in tumor tissue but not in adjacent normal kidney tissue. Therefore, the direct effects of the t(6;15) in this case might have been to trigger methylation of these CpG islands, resulting in *HACE1* silencing. Alternatively, effects on methylation due to translocation breakpoints occurring in this region may not be limited to *HACE1.* It is possible that long distance effects on expression may also affect other genes in the region, and that targeting of these genes for activation or inactivation may actually be contributing to Wilms' tumor oncogenesis rather than *HACE1.*

However, the only known genes mapping to within ~500 kb of the breakpoint include the telomeric genes *BVES*, Popeye domain containing protein 3 (*POPDC3*) and prolyl endopeptidase (*PREP*) (http://genome.ucsc.edu/). None of these genes have been implicated as oncogenes or TSGs, although this remains to be rigorously determined. No known genes are located within at least 1 Mb centromeric to the breakpoint. Interestingly, a recent reported case of Wilms' tumor with a 6q21 breakpoint maps to a 1.3 Mb region we now know includes the *HACE1* locus (9), suggesting that other rearrangements of this region may similarly occur near *HACE1* and adjacent loci in Wilms' tumor.

The 6q21 region is commonly deleted in several other human neoplasms. Examples include malignancies of the prostate, breast and ovaries, as well as leukemias and lymphomas (12–15). For example, a recent study found that ~50% of prostate cancers had deletions of the 6q21 region (15). A number of candidate metastasis suppressor genes have also been mapped to chromosome 6q21 (49). There is emerging interest in the role of protein degradation in neoplasia, and E3 ligases have been implicated in both tumor formation and suppression (50). In fact, the E6-AP HECT E3 ligase was originally defined by its ability to ubiquitinate and promote p53 degradation after recruitment by the E6 oncoprotein in HPV infected cervical carcinoma cells (23,51,52). It will be important to further assess the possibility that the Hace1 E3 ligase plays a role in human cancer.

MATERIALS AND METHODS

FISH and Southern blotting

Single color FISH was performed on metaphase and interphase nuclei from the index Wilms' tumor case. BAC probes used for mapping were obtained from the RPCI-11 human BAC library, labeled with Spectrum Green or Spectrum Red kits (Vysis) and hybridized to denatured slides as described previously (53). For Southern blotting, genomic DNA (~15 μg) extracted from frozen tissue sections was first digested with respective restriction enzymes, and then analyzed by hybridization with [α-^{32}P]dATP labeled genomic probe generated by PCR from a human DNA template SB1 (primers: forward, GGAAA CAAAA GCAAA GCGAC CCAAC TAT; reverse, GGCGG CCGAG ACCTG AGACC).

Plasmids

The *HACE1* coding region from the IMAGE cDNA clone no. 4838835 (ATCC; GenBank accession no. BC034982) was excised using *Asc*I and *Bsa*AI, blunted with T4 DNA polymerase and ligated in frame into blunted *Xho*I site of the mammalian expression vector pcDNA3–HA (Invitrogen) or pET-15b (Novagen). The HA-tagged (hemagglutinin peptide tag, YPYDVPDYA) construct was excised from pcDNA3–HA with *Sac*II, blunted with T4 DNA polymerase, and subcloned into the *Hpa*I site of pMSCV$_{hygro}$ (Clontech). To construct the plasmid encoding the Cys to Ser mutant (C876S), the 3′ *Xba*I fragment of *HACE1* was subcloned from pcDNA3-HA-Hace1 into the *Xba*I site of pBluescript-II. Site directed mutagenesis was done using the QuickChange kit (Stratagene) (primers: forward, TCAAG CACAT CCATC AACAT G; reverse, CATGT TGATG GATGT GCTTGA). The mutation was sequence verified and the *Xba*I fragment was than replaced into the original pcDNA3–HA–Hace1 construct. The N-terminal Hace1 fragment, p75, was generated by removal of a 3′ *Xba*I fragment of *HACE1* from the pET-15b–Hace1.

Cell lines

NIH3T3 cells (ATCC) were grown in Dulbecco's modified Eagle's medium (DMEM) (Invitrogen) containing 10% calf serum (CS) (Invitrogen). SK-NEP-1, SK-N-SH, SK-N-MC, HEK293 and Bosc23 cells were grown in DMEM supplemented with 10% fetal bovine serum (FBS) (Invitrogen). KCNR, SAN-2, IMR-32, Birch and CT-10 were maintained in RPMI 1640 (Invitrogen) with 15% FBS. NIH3T3 cell lines stably expressing HA–Hace1 were generated using a retroviral system as described previously (54). Briefly, ecotropic virus packaging Bosc23 cells were transfected with empty vector (pMSCV$_{hygro}$) or pMSCV$_{hygro}$–HA–Hace1 plasmid using calcium phosphate. Retrovirus-containing supernatants were collected 48 h after transfection, filtered and incubated with NIH3T3 cells for 24 h. Infected cells were selected for 4–8 days with hygromycin B (600–800 μg/ml) (Invitrogen).

Methylation assays

Methylation sensitive restriction enzyme digests followed by semi-quantitative PCR have been performed as described (55). Briefly, 100 ng of DNA, extracted from tumor and normal kidneys frozen tissue sections, was digested to completion (overnight) with *Eco*RI ± *Hae*II, *Eco*RI ± *Bss*HII or *Eco*RI ± *Hpa*II (NEB) as indicated in Figure 6. Ten nanograms of digested DNA was used for semi-quantitative PCR with amplicons surrounding CpG islands near the *HACE1* locus (Fig. 1). The 5′ region of the *MIC2* gene, previously shown to be unmethylated (56), was used as a control for complete digestion. All reactions were performed using Platinum Taq (Invitrogen) with the included buffer supplemented with 10% DMSO and carried out with the following conditions: CpG-29 (794 bp forward: GGAAA CAAAA GCAAA GCGAC CCAAC TAT, reverse: GGCGG CCGAG ACCTG AGACC, 100 nM each), 50 μM dNTPs, 1.0 mM $MgCl_2$, 94°C 30 s, 56°C 10 s, 72°C 60 s, 30 cycles. CpG-177 (804 bp, forward: TGTGC TGTTC GGAAT GATGT, reverse: CTAGC CTGGG TGTGA GAGGG, 100 nM each), 100 μM dNTPs, 1.5 mM $MgCl_2$, 94°C 45 s, 58°C 20 s, 72°C 120 s, five cycles, 94°C 30 s, 56°C 10 s, 72°C 90 s, 30 cycles. CpG-88 (939 bp, forward: CCCCG ATGCA GCTTA AAGTA, reverse: GAGGG TAGGA GGAGC AGGG, 100 nM each), 50 μM dNTPs, 1.0 mM $MgCl_2$, 94°C 45 s, 58°C 10 s, 72°C 90 s, 30 cycles. *MIC2* (512 bp, forward: AGTAT CTGTC CTGCC GCC, reverse: TTTGC AACTC CGACA ACAAA CGC, 100 nM each), 50 μM dNTPs, 1.0 mM $MgCl_2$, 94°C 45 s, 55°C 15 s, 72°C 45 s, 35 cycles. The optimal number of cycles for each reaction was determined empirically by testing a range of 25–40 cycles. Above conditions are those in which the most reproducible differences in amplification within the exponential phase of

amplification were achieved. All reactions were performed in triplicate.

To assess the effect of CpG island methylation on *HACE1* expression efficiency, SK-NEP-1 cells were treated with methylation inhibitor 5-AZ (Sigma). Treatment was done twice for 24 h over a 7-day period (on days 2 and 5) as previously described (57). DNA and RNA were isolated on day 6 and *HACE1* expression and methylation of the upstream CpG islands were assayed by qRT–PCR and semi-quantitative PCR, respectively. Each experiment was repeated four times.

Quantitative RT–PCR

Total RNA was extracted using Trizol reagent (Invitrogen) and converted to cDNA using 2 μg RNA in a random primed synthesis with the Superscript II Reverse transcriptase kit (Invitrogen). qRT–PCR was done using the TaqMan 5′ exonuclease assay. All primer/probe sets were designed to span exon boundaries to eliminate the risk of template contamination by genomic DNA and the need for DNase1 pre-treatment of RNA. *HACE1* gene specific primer/probe set (forward: TCTTA CAGTT TGTTA CGGGC AGTT, probe: [6FAM]CAAAC CCACC ATGTG GGACC CTG [TAMRA], reverse: CAATC CACTT CCACC CATGAT) was multiplexed with VIC-MGB labeled β-actin endogenous control primer/probe kit (Applied Biosystems) using TaqMan universal PCR master mix (Applied Biosystems) and standard conditions. An ABI 7000 sequence detection system (Applied Biosystems) was used to run the PCR reactions and measure fluorescence at each cycle. Generated data were further analyzed using Microsoft Excel. Each PCR reaction was performed in quadruplet and each sample was analyzed independently at least twice.

Chromatin immunoprecipitation

SK-NEP-1 or HEK293 cells were treated with or without 5 μM 5AZ as described earlier. Immunoprecipitation of DNA representing active versus inactive chromatin was performed using a ChIP assay kit (Upstate) according to the manufacturer's protocol. Briefly, DNA and protein were cross-linked in culture with 1% formaldehyde. For each reaction 1×10^6 cells were collected in 200 μl SDS lysis buffer (1% SDS, 10 mM EDTA, 50 mM Tris–HCl, pH 8.1, 1 mM PMSF, 1 μg/ml aprotinin, 1 μg/ml pepstatin A) and sonicated to shear genomic DNA to a size range of ∼300–1000 bp. Lysates were diluted 1:10 with ChIP buffer (0.01% SDS, 1.1% Triton X-100, 1.2 mM EDTA, 16.7 mM Tris–HCl, pH 8.1, 167 mM NaCl) and immunoprecipitated with the appropriate antibody overnight at 4°C with agitation. α-Acetyl-histone H3 (Lys9/Lys14) antibodies (Upstate) were used to immunoprecipitate active chromatin fragments (58), whereas α-dimethyl-histone H3 (Lys79) antibodies (Upstate) were used to immunoprecipitate inactive chromatin (35) with protein A beads. Protein A agarose/Salmon sperm DNA slurry (Upstate) added to lysates without antibody was used as a negative control (data not shown). DNA was recovered by proteinase K digestion and phenol/chloroform extraction after washing and reversal of cross-links. Equal volumes were utilized to maintain the quantitative nature of the assay. The recovered DNA pellet was air dried and resuspended in 25 μl of TE (10 mM Tris–HCl, 1 mM EDTA, pH 8.0). Immunoprecipitated *HACE1* levels were determined by using PCR amplifying the 5′ end of the gene, overlapping the CpG-88 island. PCR was carried out with Platinum Taq (Invitrogen) with the included buffer, supplemented with 10% DMSO and the following conditions: 2.5 μl recovered ChIP DNA, primers (297 bp product, forward: CGGCT CACCC TCGGG CAACT CC, reverse: CGGCG GCGGG TGTAC TGTAG GTGGT C, 200 nM each), 100 μM dNTPs, 2 mM $MgCl_2$, 94°C 30 s, 55°C 30 s, 72°C 45 s, 32 cycles. Input DNA amounts were verified by PCR using the same conditions as mentioned using DNA extracted from a 100 μl aliquot of 'ChIP buffer' diluted cell lysate taken prior to addition of antibodies, as recommended by the ChIP assay kit (Upstate) (shown as 'input fraction' in Fig. 6D). Input was also verified with 2.5 μl of recovered immunoprecipitated DNA using the a PCR assay for 5′ end of the unmethylated *MIC2* gene (55,56), as described earlier (data not shown). The optimal number of cycles for each reaction was determined empirically by testing a range of 25–40 cycles. The conditions mentioned earlier are those in which the most reproducible differences in amplification within the exponential phase of amplification were achieved. The entire ChIP experiment was repeated four times for each cell line.

Sequence analysis

Genomic DNA from Wilms' tumors, patient-matched normal kidney (same cohort used for expression analysis) and the SK-NEP-1 cell line were used as templates for sequencing. Reference sequence for primer design, exon layout and assembly was obtained from the UCSC human genome database (http://genome.ucsc.edu/). Forward and reverse primers for each of the 24 *HACE1* exons contained the 21M13F (TGTAAAACGACGGCCAGT) or M13R (CAGGAAACAGCTATGAC) sequences at their 5′ ends, respectively. After PCR of each exon from genomic DNA samples automated sequencing was performed by standard methods. Sequence reads were base-called using Phred software and subsequently assembled with reference sequences using Phrap software (59,60). Contigs of sequence traces corresponding to each exon were examined using PolyPhred software (61) for detection of heterozygotes and visualized in Consed software (62) to facilitate verification of sequence variants by examination of individual traces.

Thioester bond formation assay

L-[^{35}S]-Methionine labeled Hace1 proteins were synthesized *in vitro* in a coupled transcription/translation system (Promega) using pcDNA3-HA–Hace1 plasmids coding for the wild-type and mutant Hace1 proteins. Reaction mixtures contained 2 μl of the translation reaction, GST–Ub (1 μg), 50 mM KCl, 5 mM $MgCl_2$, 2 mM ATP, 10 mM creatine phosphate, 0.5 U of creatine phosphokinase, 1 mM DTT, and 20 mM Tris–HCl (pH 7.8). Reactions were also supplemented with E1 (∼0.5 μg) and the respective E2s (∼0.4 μg) (Boston-Biochem). After incubation for 30 min at 30°C, reactions were stopped with 2 × SDS–PAGE sample buffer at the

absence or presence of 300 mM β-mercaptoethanol. Reactions containing β-mercaptoethanol were then boiled for 3 min, and those lacking β-mercaptoethanol were incubated at room temperature for 20 min before loading. Reaction products were resolved by SDS–7% PAGE and visualized by autoradiography.

Purification of the recombinant proteins from bacteria and antibody preparation

Hace1 or p75, lacking the HECT domain, were expressed as His-tagged fusion proteins in *Escherichia coli* BL21(DE3). After 4 h of IPTG induction, bacteria were lysed by sonication in buffer containing 2 M NaCl, 10 mM Tris–HCl (pH 7.6) and 0.5 mM PMSF. Cell debris was removed by centrifugation at 10 000*g* for 20 min at 4°C. The supernatant was diluted 4-fold with 10 mM Tris–HCl (pH 7.6), 0.5 mM PMSF and passed through a Ni^{+}–Sepharose column (Qiagen). After washing the column with loading buffer [500 mM NaCl, 10 mM Tris–HCl (pH 7.6)], bound proteins were eluted with the same buffer containing 300 mM imidazole and dialyzed against 200 mM KCl, 10 mM Tris–HCl (pH 7.6). α-Hace1 antibodies were generated by subcutaneous immunization of rabbits with the full-length Hace1 recombinant protein or with the N-terminal Hace1 peptide (CLVLL LKKGA NPNYQ DISG) and used for western blotting at 1:2000 dilution.

Immunoprecipitation and western blotting

Immunoprecipitation and western blotting were done essentially as described previously (53,63). Briefly, immunoprecipitations were performed using 500 μl of cytoplasmic cell extracts (~500 μg–1 mg of total protein) and 3 μl (~3 μg) of the appropriate antibodies immobilized on 20 μl of protein (A + G)–Sepharose beads (Qiagen) for 2–3 h at 4°C with rotation. For immunoprecipitation of 26S proteasome, the mixture of antibodies directed against α and β subunits [Calbiochem; 5 μl of each antibody per 30 μl of protein(A)–Sepharose] has been used. Monoclonal mouse α-HA (Babco), α-BiP, α-Grb2 and α-UbcH7 (Transduction Laboratories), α-p97 (VCP; Research Diagnostics Inc.), goat α-actin, rabbit α-Ub (Santa Cruz) and α-acetyl-histone H3 (Upstate) antibodies were used at 1:1000 dilution.

Subcellular fractionation

To prepare cell extracts, NIH3T3 cells expressing HA-Hace1 were trypsinized, washed three times with PBS and lysed with buffer containing 50 mM KCl, 2 mM $MgCl_2$, 2 mM DTT, 0.25% NP-40, 20 mM Hepes–KOH (pH 7.8) and the proteasome inhibitors MG132 (20 μM) or lactacystin (10 μM). Nuclear, mitochondrial and post-mitochondrial fractions were separated by sequential centrifugation at 1000*g* for 5 min followed by centrifugation at 10 000*g* for 15 min. Nuclei were then additionally purified from the re-suspended 1000*g* pellet fraction by spinning down through a 50% glycerol cushion. The post-ribosomal supernatant was obtained by a further 20 min centrifugation of the post-mitochondrial fraction at 100 000 rpm in a TLA-100 centrifuge (Beckman). Cell fractions were normalized for protein concentration using Protein Assay kit (BioRad).

Immunofluorescence microscopy

NIH3T3 cells exponentially growing on coverslips were rinsed with PBS and fixed with −20°C cold methanol for 10 min. To detect Hace1 and BiP, coverslips were incubated overnight with a mixture of rabbit α-Hace1 (1:2000 dilution) and mouse α-BiP antibodies (1:1000 dilution) followed by the secondary antibodies Rhodamine Red-X-conjugated goat α-rabbit and Oregon Green 514-conjugated goat α-mouse (Molecular Probes). Slides were counterstained with DAPI and analyzed using a Zeiss Axioplan epifluorescent microscope equipped with a COHU-CCD camera. Control staining with pre-immune antibodies or no primary antibodies showed no signal (data not shown).

SUPPLEMENTARY MATERIAL

Supplementary Material is available at HMG Online.

ACKNOWLEDGEMENTS

We would like to thank Seong-Jin Kim for reagents, Joan Mathers and Heather Wildgrove for technical assistance, Francis Ouellette, Yaron Butterfield, Jacqueline Schein, Stefanie Butland and Sohrab Shah for bioinformatics support, as well as Fred Barr, Catherine Anderson, Lola Maksumova, Gregor Reid and Fan Zhang for helpful discussions. Normal fetal kidney samples were provided by Alan G. Fantel, Birth Defects Research Laboratory, University of Washington. This study was supported by the National Cancer Institute of Canada and by a Translational Research Grant from the Children's Oncology Group (to P.H.B.S.). This work was also funded by the Johal Program in Pediatric Oncology Basic and Translational Research at the BC Research Institute for Children's and Women's Health.

REFERENCES

1. Rabbitts, T.H. (1994) Chromosomal translocations in human cancer. *Nature*, **372**, 143–149.
2. Gnarra, J.R., Tory, K., Weng, Y., Schmidt, L., Wei, M.H., Li, H., Latif, F., Liu, S., Chen, F., Duh, F.M. *et al.* (1994) Mutations of the VHL tumor suppressor gene in renal carcinoma. *Nat. Genet.*, **7**, 85–90.
3. Arai, E., Ikeuchi, T. and Nakamura, Y. (1994) Characterization of the translocation breakpoint on chromosome 22q12.2 in a patient with neurofibromatosis type 2 (NF2). *Hum. Mol. Genet.*, **3**, 937–939.
4. Rosty, C., Peter, M., Zucman, J., Validire, P., Delattre, O. and Aurias, A. (1998) Cytogenetic and molecular analysis of a t(1;22)(p36;q11.2) in a rhabdoid tumor with a putative homozygous deletion of chromosome 22. *Genes Chromosomes Cancer*, **21**, 82–89.
5. Versteege, I., Sevenet, N., Lange, J., Rousseau-Merck, M.F., Ambros, P., Handgretinger, R., Aurias, A. and Delattre, O. (1998) Truncating mutations of hSNF5/INI1 in aggressive paediatric cancer. *Nature*, **394**, 203–206.
6. Martin, E.S., Cesari, R., Pentimalli, F., Yoder, K., Fishel, R., Himelstein, A.L., Martin, S.E., Godwin, A.K., Negrini, M. and Croce, C.M. (2003) The BCSC-1 locus at chromosome 11q23–q24 is a candidate tumor suppressor gene. *Proc. Natl Acad. Sci. USA*, **100**, 11517–11522.

7. Fernandez, C.V., Lestou, V.S., Wildish, J., Lee, C.L. and Sorensen, P.H. (2001) Detection of a novel t(6;15)(q21;q21) in a pediatric Wilms tumor. *Cancer Genet. Cytogenet.*, **129**, 165–167.
8. Dome, J.S. and Coppes, M.J. (2002) Recent advances in Wilms tumor genetics. *Curr. Opin. Pediatr.*, **14**, 5–11.
9. Bruce, C.K., Howard, P., Nowak, N.J. and Hoban, P.R. (2003) Molecular analysis of region t(5;6)(q21;q21) in Wilms tumor. *Cancer Genet. Cytogenet.*, **141**, 106–113.
10. Hoban, P.R., Cowen, R.L., Mitchell, E.L., Evans, D.G., Kelly, M., Howard, P.J. and Heighway, J. (1997) Physical localisation of the breakpoints of a constitutional translocation t(5;6)(q21;q21) in a child with bilateral Wilms' tumor. *J. Med. Genet.*, **34**, 343–345.
11. Solis, V., Pritchard, J. and Cowell, J.K. (1988) Cytogenetic changes in Wilms' tumors. *Cancer Genet. Cytogenet.*, **34**, 223–234.
12. Utada, Y., Haga, S., Kajiwara, T., Kasumi, F., Sakamoto, G., Nakamura, Y. and Emi, M. (2000) Mapping of target regions of allelic loss in primary breast cancers to 1-cM intervals on genomic contigs at 6q21 and 6q25.3. *Jpn J. Cancer Res.*, **91**, 293–300.
13. Zhang, Y., Matthiesen, P., Harder, S., Siebert, R., Castoldi, G., Calasanz, M.J., Wong, K.F., Rosenwald, A., Ott, G., Atkin, N.B. *et al.* (2000) A 3-cM commonly deleted region in 6q21 in leukemias and lymphomas delineated by fluorescence *in situ* hybridization. *Genes Chromosomes Cancer*, **27**, 52–58.
14. Orphanos, V., McGown, G., Hey, Y., Thorncroft, M., Santibanez-Koref, M., Russell, S.E., Hickey, I., Atkinson, R.J. and Boyle, J.M. (1995) Allelic imbalance of chromosome 6q in ovarian tumors. *Br. J. Cancer*, **71**, 666–669.
15. Hyytinen, E.R., Saadut, R., Chen, C., Paull, L., Koivisto, P.A., Vessella, R.L., Frierson, H.F., Jr and Dong, J.T. (2002) Defining the region(s) of deletion at 6q16–q22 in human prostate cancer. *Genes Chromosomes Cancer*, **34**, 306–312.
16. Morelli, C., Karayianni, E., Magnanini, C., Mungall, A.J., Thorland, E., Negrini, M., Smith, D.I. and Barbanti-Brodano, G. (2002) Cloning and characterization of the common fragile site FRA6F harboring a replicative senescence gene and frequently deleted in human tumors. *Oncogene*, **21**, 7266–7276.
17. Pickart, C.M. (2001) Mechanisms underlying ubiquitination. *Annu. Rev. Biochem.*, **70**, 503–533.
18. Huibregtse, J.M., Scheffner, M., Beaudenon, S. and Howley, P.M. (1995) A family of proteins structurally and functionally related to the E6-AP ubiquitin-protein ligase. *Proc. Natl Acad. Sci. USA*, **92**, 2563–2567.
19. Weissman, A.M. (2001) Themes and variations on ubiquitylation. *Nat. Rev. Mol. Cell. Biol.*, **2**, 169–178.
20. Bork, P. (1993) Hundreds of ankyrin-like repeats in functionally diverse proteins: mobile modules that cross phyla horizontally? *Proteins*, **17**, 363–374.
21. Ingham, R.J., Gish, G. and Pawson, T. (2004) The Nedd4 family of E3 ubiquitin ligases: functional diversity within a common modular architecture. *Oncogene*, **23**, 1972–1984.
22. Arcellana-Panlilio, M.Y., Egeler, R.M., Ujack, E., Pinto, A., Demetrick, D.J., Robbins, S.M. and Coppes, M.J. (2000) Decreased expression of the INK4 family of cyclin-dependent kinase inhibitors in Wilms tumor. *Genes Chromosomes Cancer*, **29**, 63–69.
23. Huibregtse, J.M., Scheffner, M. and Howley, P.M. (1993) Cloning and expression of the cDNA for E6-AP, a protein that mediates the interaction of the human papillomavirus E6 oncoprotein with p53. *Mol. Cell. Biol.*, **13**, 775–784.
24. Izzi, L. and Attisano, L. (2004) Regulation of the TGFbeta signalling pathway by ubiquitin-mediated degradation. *Oncogene*, **23**, 2071–2078.
25. Horster, M.F., Braun, G.S. and Huber, S.M. (1999) Embryonic renal epithelia: induction, nephrogenesis, and cell differentiation. *Physiol. Rev.*, **79**, 1157–1191.
26. Pritchard-Jones, K. and Hastie, N.D. (1990) Wilms' tumor as a paradigm for the relationship of cancer to development. *Cancer Surv.*, **9**, 555–578.
27. Pritchard-Jones, K. (1999) The Wilms tumor gene, WT1, in normal and abnormal nephrogenesis. *Pediatr. Nephrol.*, **13**, 620–625.
28. Coppes, M.J. and Pritchard-Jones, K. (2000) Principles of Wilms' tumor biology. *Urol. Clin. North Am.*, **27**, 423–433, viii.
29. Knudson, A.J. and Strong, L.C. (1972) Mutation and cancer: a model for Wilms' tumor of the kidney. *J. Natl Cancer Inst.*, **48**, 313–324.
30. Jones, P.A. and Baylin, S.B. (2002) The fundamental role of epigenetic events in cancer. *Nat. Rev. Genet.*, **3**, 415–428.
31. Jain, P.K. (2003) Epigenetics: the role of methylation in the mechanism of action of tumor suppressor genes. *Ann. NY Acad. Sci.*, **983**, 71–83.
32. Nephew, K.P. and Huang, T.H. (2003) Epigenetic gene silencing in cancer initiation and progression. *Cancer Lett.*, **190**, 125–133.
33. Momparler, R.L. and Bovenzi, V. (2000) DNA methylation and cancer. *J. Cell. Physiol.*, **183**, 145–154.
34. Jones, P.A. and Taylor, S.M. (1980) Cellular differentiation, cytidine analogs and DNA methylation. *Cell*, **20**, 85–93.
35. Ng, H.H., Feng, Q., Wang, H., Erdjument-Bromage, H., Tempst, P., Zhang, Y. and Struhl, K. (2002) Lysine methylation within the globular domain of histone H3 by Dot1 is important for telomeric silencing and Sir protein association. *Genes Dev.*, **16**, 1518–1527.
36. Iizuka, M. and Smith, M.M. (2003) Functional consequences of histone modifications. *Curr. Opin. Genet. Dev.*, **13**, 154–160.
37. Berger, S.L. (2002) Histone modifications in transcriptional regulation. *Curr. Opin. Genet. Dev.*, **12**, 142–148.
38. Friedlander, R., Jarosch, E., Urban, J., Volkwein, C. and Sommer, T. (2000) A regulatory link between ER-associated protein degradation and the unfolded-protein response. *Nat. Cell Biol.*, **2**, 379–384.
39. Russo, A.A., Tong, L., Lee, J.O., Jeffrey, P.D. and Pavletich, N.P. (1998) Structural basis for inhibition of the cyclin-dependent kinase Cdk6 by the tumor suppressor p16INK4a. *Nature*, **395**, 237–243.
40. Rice, J.C., Ozcelik, H., Maxeiner, P., Andrulis, I. and Futscher, B.W. (2000) Methylation of the BRCA1 promoter is associated with decreased BRCA1 mRNA levels in clinical breast cancer specimens. *Carcinogenesis*, **21**, 1761–1765.
41. Nguyen, C., Liang, G., Nguyen, T.T., Tsao-Wei, D., Groshen, S., Lubbert, M., Zhou, J.H., Benedict, W.F. and Jones, P.A. (2001) Susceptibility of nonpromoter CpG islands to *de novo* methylation in normal and neoplastic cells. *J. Natl Cancer Inst.*, **93**, 1465–1472.
42. Srivastava, M., Hsieh, S., Grinberg, A., Williams-Simons, L., Huang, S.P. and Pfeifer, K. (2000) H19 and Igf2 monoallelic expression is regulated in two distinct ways by a shared cis acting regulatory region upstream of H19. *Genes Dev.*, **14**, 1186–1195.
43. Ginjala, V., Holmgren, C., Ulleras, E., Kanduri, C., Pant, V., Lobanenkov, V., Franklin, G. and Ohlsson, R. (2002) Multiple cis elements within the Igf2/H19 insulator domain organize a distance-dependent silencer. A cautionary note. *J. Biol. Chem.*, **277**, 5707–5710.
44. Roessler, E., Ward, D.E., Gaudenz, K., Belloni, E., Scherer, S.W., Donnai, D., Siegel-Bartelt, J., Tsui, L.C. and Muenke, M. (1997) Cytogenetic rearrangements involving the loss of the Sonic Hedgehog gene at 7q36 cause holoprosencephaly. *Hum. Genet.*, **100**, 172–181.
45. Belloni, E., Muenke, M., Roessler, E., Traverso, G., Siegel-Bartelt, J., Frumkin, A., Mitchell, H.F., Donis-Keller, H., Helms, C., Hing, A.V. *et al.* (1996) Identification of Sonic hedgehog as a candidate gene responsible for holoprosencephaly. *Nat. Genet.*, **14**, 353–356.
46. Grewal, S.I. and Moazed, D. (2003) Heterochromatin and epigenetic control of gene expression. *Science*, **301** 798–802.
47. Noma, K., Allis, C.D. and Grewal, S.I. (2001) Transitions in distinct histone H3 methylation patterns at the heterochromatin domain boundaries. *Science*, **293**, 1150–1155.
48. Richards, E.J. and Elgin, S.C. (2002) Epigenetic codes for heterochromatin formation and silencing: rounding up the usual suspects. *Cell*, **108**, 489–500.
49. Yoshida, B.A., Sokoloff, M.M., Welch, D.R. and Rinker-Schaeffer, C.W. (2000) Metastasis-suppressor genes: a review and perspective on an emerging field. *J. Natl Cancer Inst.*, **92**, 1717–1730.
50. Sakamoto, K.M. (2002) Ubiquitin-dependent proteolysis: its role in human diseases and the design of therapeutic strategies. *Mol. Genet. Metab.*, **77**, 44–56.
51. Scheffner, M., Huibregtse, J.M., Vierstra, R.D. and Howley, P.M. (1993) The HPV-16 E6 and E6-AP complex functions as a ubiquitin-protein ligase in the ubiquitination of p53. *Cell*, **75**, 495–505.
52. Yang, Y., Li, C.C. and Weissman, A.M. (2004) Regulating the p53 system through ubiquitination. *Oncogene*, **23**, 2096–2106.
53. Tognon, C., Knezevich, S.R., Huntsman, D., Roskelley, C.D., Melnyk, N., Mathers, J.A., Becker, L., Carneiro, F., MacPherson, N., Horsman, D. *et al.* (2002) Expression of the ETV6–NTRK3 gene fusion as a primary event in human secretory breast carcinoma. *Cancer Cell*, **2**, 367–376.
54. Tognon, C.E., Kirk, H.E., Passmore, L.A., Whitehead, I.P., Der, C.J. and Kay, R.J. (1998) Regulation of RasGRP via a phorbol ester-responsive C1 domain. *Mol. Cell. Biol.*, **18**, 6995–7008.

55. Anderson, C.L. and Brown, C.J. (2002) Variability of X chromosome inactivation: effect on levels of TIMP1 RNA and role of DNA methylation. *Hum. Genet.*, **110**, 271–278.
56. Goodfellow, P.J., Mondello, C., Darling, S.M., Pym, B., Little, P. and Goodfellow, P.N. (1988) Absence of methylation of a CpG-rich region at the 5′ end of the MIC2 gene on the active X, the inactive X, and the Y chromosome. *Proc. Natl Acad. Sci. USA*, **85**, 5605–5609.
57. Sarkar, S., Roy, B.C., Hatano, N., Aoyagi, T., Gohji, K. and Kiyama, R. (2002) A novel ankyrin repeat-containing gene (Kank) located at 9p24 is a growth suppressor of renal cell carcinoma. *J. Biol. Chem.*, **277**, 36585–36591.
58. Luo, R.X., Postigo, A.A. and Dean, D.C. (1998) Rb interacts with histone deacetylase to repress transcription. *Cell*, **92**, 463–473.
59. Ewing, B. and Green, P. (1998) Base-calling of automated sequencer traces using phred. II. Error probabilities. *Genome Res.*, **8**, 186–194.
60. Ewing, B., Hillier, L., Wendl, M.C. and Green, P. (1998) Base-calling of automated sequencer traces using phred. I. Accuracy assessment. *Genome Res.*, **8**, 175–185.
61. Nickerson, D.A., Tobe, V.O. and Taylor, S.L. (1997) PolyPhred: automating the detection and genotyping of single nucleotide substitutions using fluorescence-based resequencing. *Nucl. Acids Res.*, **25**, 2745–2751.
62. Gordon, D., Abajian, C. and Green, P. (1998) Consed: a graphical tool for sequence finishing. *Genome Res.*, **8**, 195–202.
63. Evdokimova, V., Ruzanov, P., Imataka, H., Raught, B., Svitkin, Y., Ovchinnikov, L.P. and Sonenberg, N. (2001) The major mRNA-associated protein YB-1 is a potent 5′ cap-dependent mRNA stabilizer. *EMBO J.*, **20**, 5491–5502.